ICARUS 56, 15–37 (1983)

Martian Rampart Crater Ejecta: Experiments and Analysis of Melt–Water Interaction[1]

K. H. WOHLETZ* AND M. F. SHERIDAN†

*Earth and Space Science Division, Los Alamos National Laboratory, Los Alamos, New Mexico 87545 and †Department of Geology, Arizona State University, Tempe, Arizona 85276

Received October 18, 1982; revised May 31, 1983

Viking images of Martian craters with rampart-bordered ejecta deposits reveal distinct impact ejecta morphology when compared to that associated with similar-sized craters on the Moon and Mercury. Topographic control of distribution, lobate and terraced margins, cross-cutting relationships, and multiple stratigraphic units are evidence for ejecta emplacement by surface flowage. It is suggested that target water explosively vaporized during impact alters initial ballistic trajectories of ejecta and produces surging flow emplacement. The dispersal of particulates during a series of controlled steam explosions generated by interaction of a thermite melt with water has been experimentally modeled. Preliminary results indicate that the mass ratio of water to melt and confining pressure control the degree of melt fragmentation (ejecta particle size) and the energy and mode of melt-ejecta dispersal. Study of terrestrial, lobate, volcanic ejecta produced by steam-blast explosions reveals that particle size and vapor to clast volume ratio are primary parameters characterizing the emplacement mechanism and deposit morphology. Martian crater ramparts are formed when ejecta surges lose fluidizing vapors and transported particles are deposited en masse. This deposition results from flow yield strength increasing above shear stress due to interparticle friction.

INTRODUCTION

Studies by Head and Roth (1976) and Carr *et al.* (1977) of Viking imagery point out that ejecta deposits surrounding large, Martian impact craters, up to 50 km in diameter, are different from those around similar-sized craters on the Moon and Mercury. The Martian craters are surrounded by lobate or multilobate ejecta deposits and have been termed "splosh," "fluidized," "rampart," or "pedestal" craters (Mutch and Worronow, 1980; Mouginis-Mark, 1979a). Their deposits appear to have been emplaced by ejecta flow over the surface away from the crater. The presence of abundant surface or near-surface water early in Martian history is indicated by considerable evidence (Toulmin *et al.*, 1977; Carr and Schaber, 1977). Therefore, water is an important factor for consideration when comparing the lobate ejecta patterns of Mars to the simple ballistic patterns on the Moon and Mercury, where the environment has been essentially water free (Cintala and Mouginis-Mark, 1980). To better understand the relationship of target water to ejecta morphology, Johansen (1979), Mouginis-Mark (1979a), and Blasius and Cutts (1980) attempt to correlate morphology variation with latitude, elevation, and target lithology. However, the interpretation of morphology statistics has been limited by a lack of both information concerning distribution of water on the surface of Mars as well as a generally accepted model explaining formation of lobate ejecta deposits.

A few recent papers relate water content of target material to crater formation, dispersal of products, and types of deposits. Gault and Greeley (1978) and Greeley *et al.* (1980) impacted targets of varying water

[1] This work was performed under the auspices of the U.S. Department of Energy.

0019-1035/83 $3.00

content using the NASA–Ames Research Center vertical gun. Preliminary results indicate a strong effect on crater and ejecta deposit morphology by yield strength and viscosity, which are dependent on water content. Kieffer and Simonds (1980), in their review of the literature on terrestrial impact structures, have shown that although impact melt is more readily formed in lithologies rich in volatiles, melts associated with such targets are widely dispersed from their craters by rapid volatile expansion. Hence dry terrestrial targets contain thick melt sheets, whereas wet targets lack melt sheets but are surrounded by suevite blankets.

This paper describes possible effects that explosive water vaporization might have on ejecta emplacement after impact into a wet target. A general model (Fig. 1) is formulated from analysis of Viking imagery and experimental vapor explosions as well as consideration of fluidized particulate transport and lobate volcanic deposits. The model contends that as target water content increases, the effects of vapor expansion due to impact increasingly modify the ballistic flow field during crater excavation. This modification results in transport by gravity driven surface flowage, and is similar to that of atmospheric drag effects on ejecta modeled by Schultz and Gault (1979).

Critical to this problem is the mechanism by which water and impact melt become intimately intermixed so that efficient energy transfer is possible. We consider several other situations of melt–water interaction, albeit quite different physically, however, instructive in the dynamics of vapor explosions. The dynamic interaction of molten materials and water has been studied by numerous workers concerned with vapor explosions at foundaries (Lipsett, 1966). The literature on such industrial melt-coolant explosions is summarized by Sandia Laboratories (1975). Another source of data comes from natural steam explosions which are common in terrestrial volcanoes where magma interacts with near-surface water (Colgate and Sigurgeirsson, 1973; Peckover *et al.*, 1973; Wohletz, 1980; Sheridan and Wohletz, 1981). Numerous papers describe the phenomenology and products of such hydromagmatic eruptions as reviewed by Wohletz and Sheridan (1983). Usually flash vaporation leads to strong fragmentation of the melt; dispersal of ejecta from the explosion center is by ground-hugging, partly fluidized density currents termed surges (Moore, 1966; Waters and Fisher, 1971; Wohletz and Sheridan, 1979).

Also of importance to ejecta emplacement is the affect of shock waves. The affect of shock waves on the atmospheric flow field produced by the projectile bow shock, vapor explosion, or other mechanism is complex and beyond the scope of this paper (see Jones and Kodis, 1982; Schultz and Gault, 1982). It is worthwhile to note, however, that the experimental work to be discussed indicates that shock phenomena trigger and enhance vapor explosion processes.

VIKING IMAGERY DESCRIPTION

Observations of Martian rampart crater deposits based on interpretation of Viking imagery form the principal constraints on our models of ejecta emplacement. Twelve Martian rampart craters were studied to quantitatively characterize their deposit morphology. Maps of three of the craters (Figs. 2–4) are presented to show representative deposit characteristics, aereal extent of depositional units, and spatial relationships of rampart lobes. The following map units are based in part on interpretations of Mouginis-Mark (1978, 1979b).

Wall material (*W*). This material comprises deposits that form discontinuous, concentric scarp ridges parallel to the circumference rim on the inner slopes of craters. Some craters have multiple rings of wall material that form concentric tilted terraces. The inward decrease in elevation of multiple ridges suggests an origin by col-

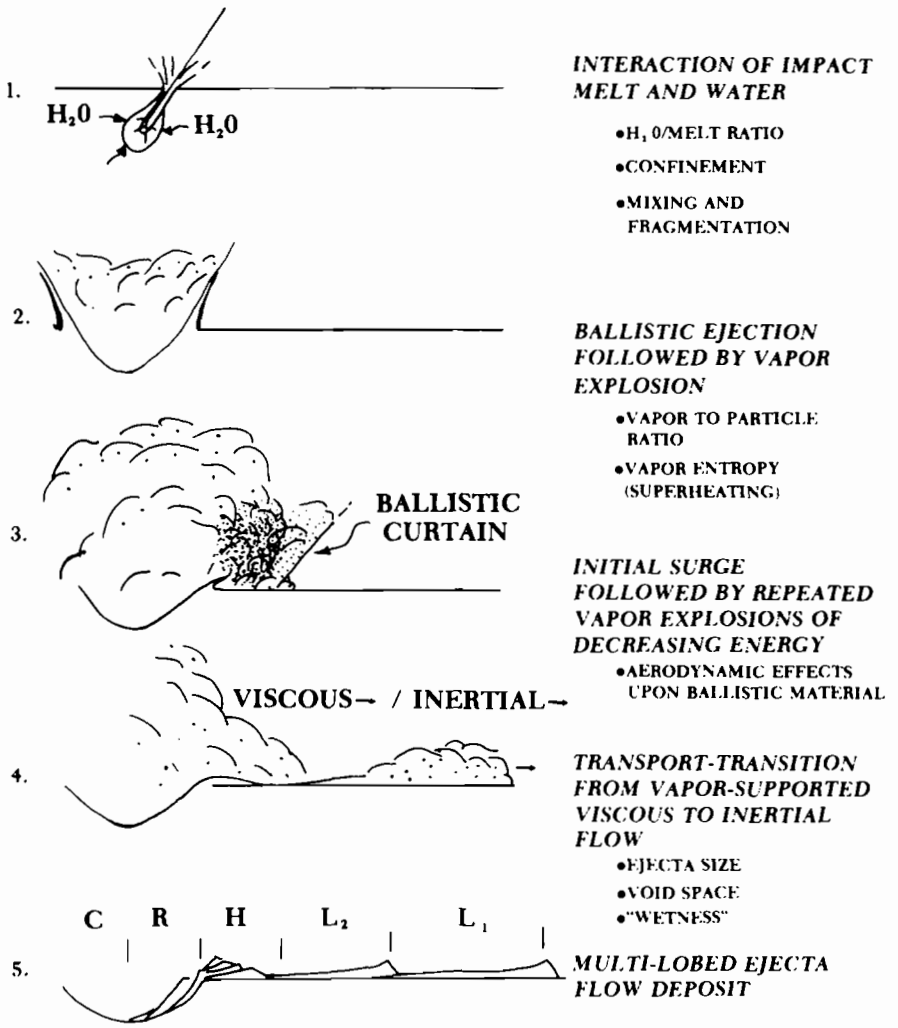

FIG. 1. Schematic model of rampart ejecta emplacement.

lapse of slump blocks. Such terraces are common in large impact craters regardless of whether the target was dry, such as the Moon or Mercury, or volatile rich, as appears to be the case for many Martian craters. We suggest that in a volatile-rich environment these features could also be explained by rapid, local withdrawal of support related to vapor explosions in the crater during and shortly after initial excavation. Terrestrial analogs of such features are common within maar craters produced by hydrovolcanic steam-blast explosions (Lorenz, 1970).

Hummocky material (*H*). The outer slopes of rampart crater rims are characterized by hummocky ridged material that extends out to the surrounding plain. This material resembles short and stubby stacked plates or "shingles" of ejecta layers that may be related to an overturned flap of rim materials. Multiple layers are likely the result of excavation through a crustal stratigraphy composed of several different lithologic units.

Lobate ejecta (*L*). These relatively thin ejecta sheets extend beyond the hummocky material to the limits of continuous ejecta.

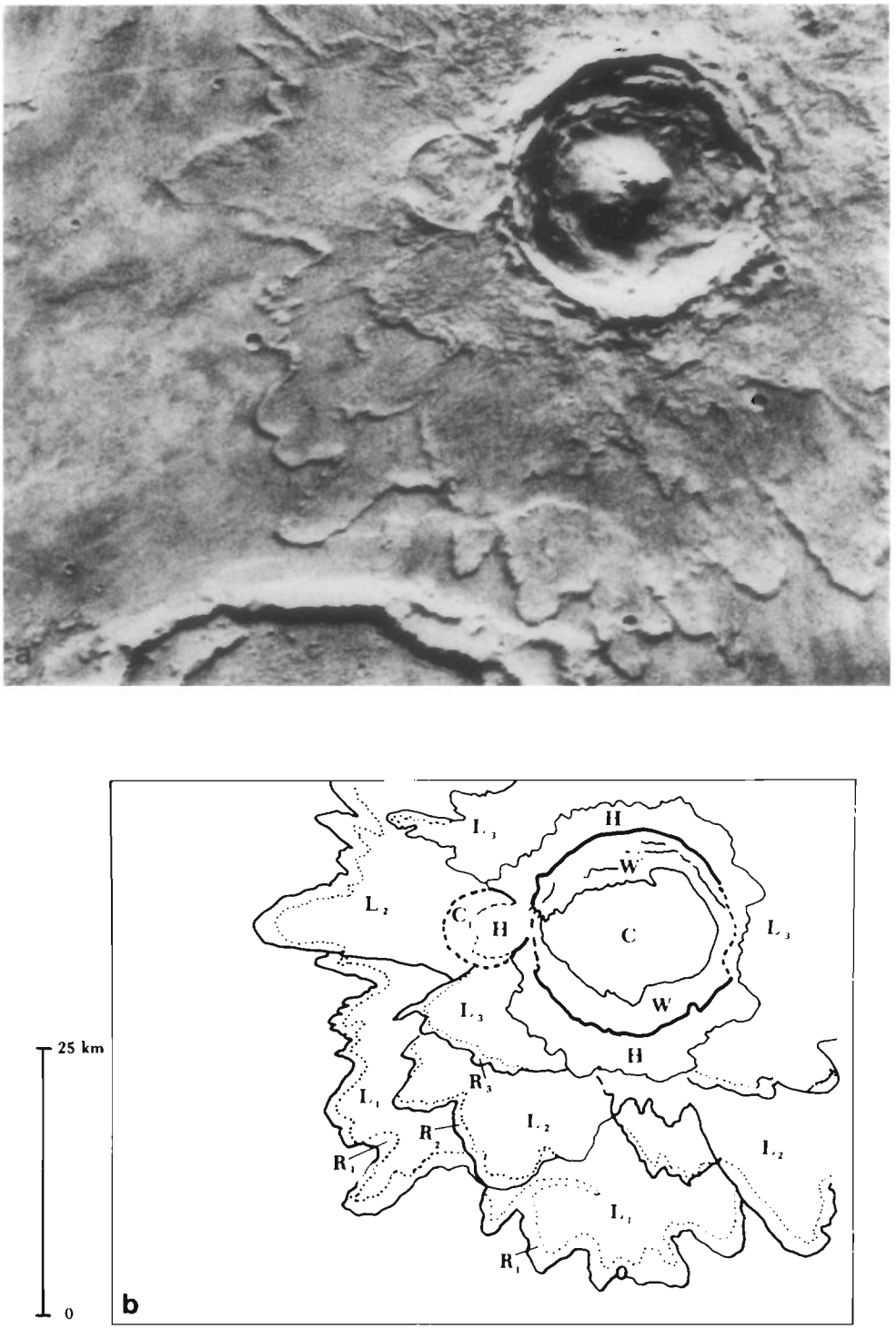

FIG. 2. Paired photo (a) and map (b) of Yuty crater, C, showing multiple lobes of rampart ejecta sheets. Note the topographic effect of crater, C_1, on the dispersal pattern of L_3 and H. Unit terminology and descriptions are given in the text. Viking image 003A07.

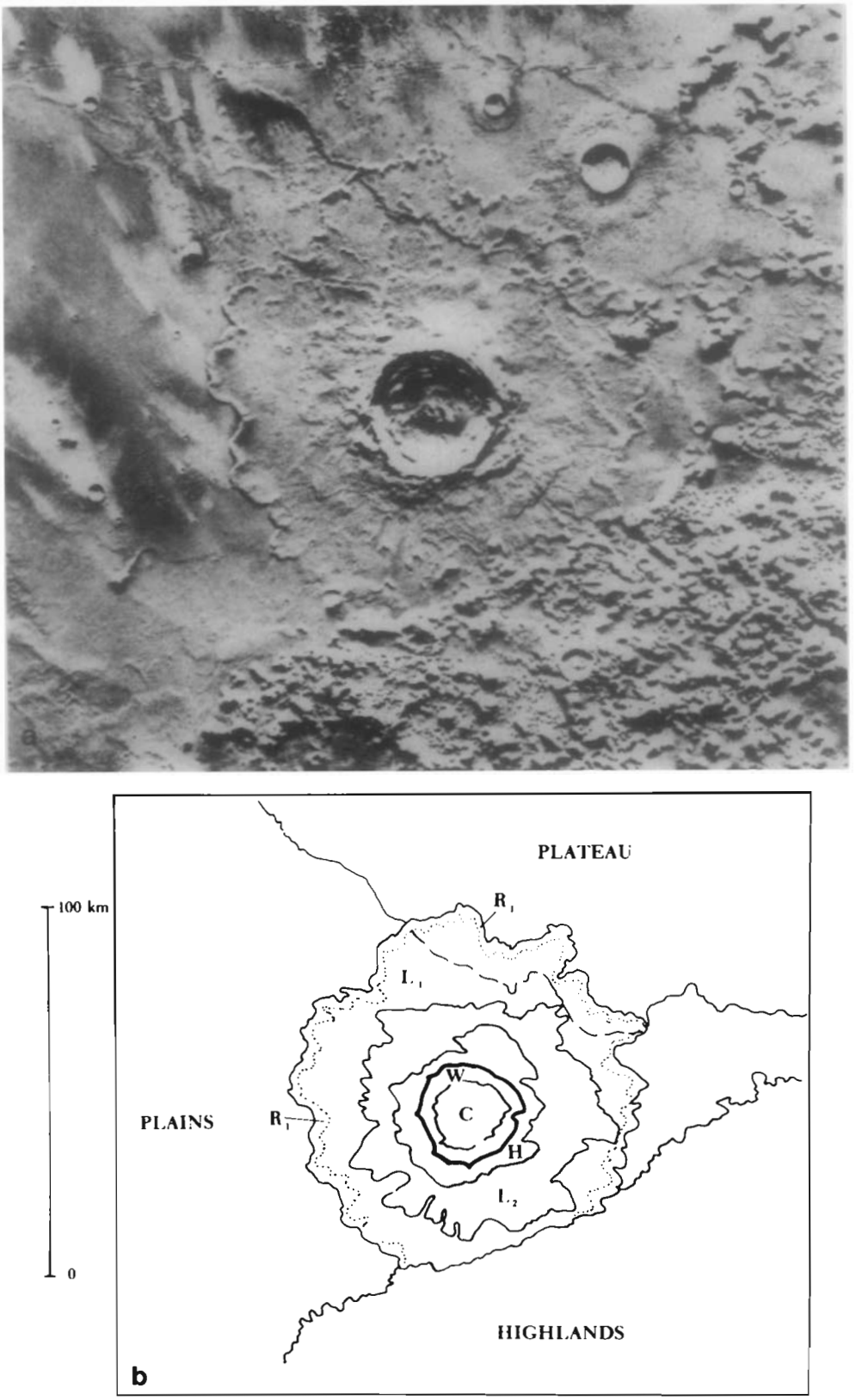

FIG. 3. Paired photo (a) and map (b) showing the constraint of rampart ejecta by highland topography. The plateau to the top was insufficient to block flowage of the lobe. Viking image 545A30.

In plan view, individual lobe terminations have a tongue-like shape with the apex pointing away from the crater. Interconnected distal lobes define a scalloped but continuous outer margin of ejecta flows. Concentric lobes are here designated by numerical subscripts; subscript 1 applies to the lobe set of greatest runout distance and successive lobe sets of lesser runout distance are designated by subscripts 2 and 3.

Ramparts (R). Some lobes have a terminal scarp which is marked by either a flat ridge or a gradual increase in deposit thickness. These ramparts have steep outer walls that mark step-like boundaries for flow lobes. The raised rim distinguishes rampart deposits from pedestal deposits that resemble an overturned saucer.

The observed stratigraphic relationships of ejecta deposits outline some constraints for a ejecta emplacement model. These relationships are discussed below.

Ejecta lobes (L_1 and L_2) from Yuty crater (C) shown in Figs. 2a and b have overrun a nearby older crater (C_1). However, a later flow lobe (L_3) has deflected around the raised rim of C_1 and is locally covered by the hummocky deposits (H). Cross-cutting relationships of ramparts indicate that the ejecta lobes were emplaced in a general sequence: L_1, L_2, and L_3 followed by H. The fact that L_1 and L_2 have passed over the

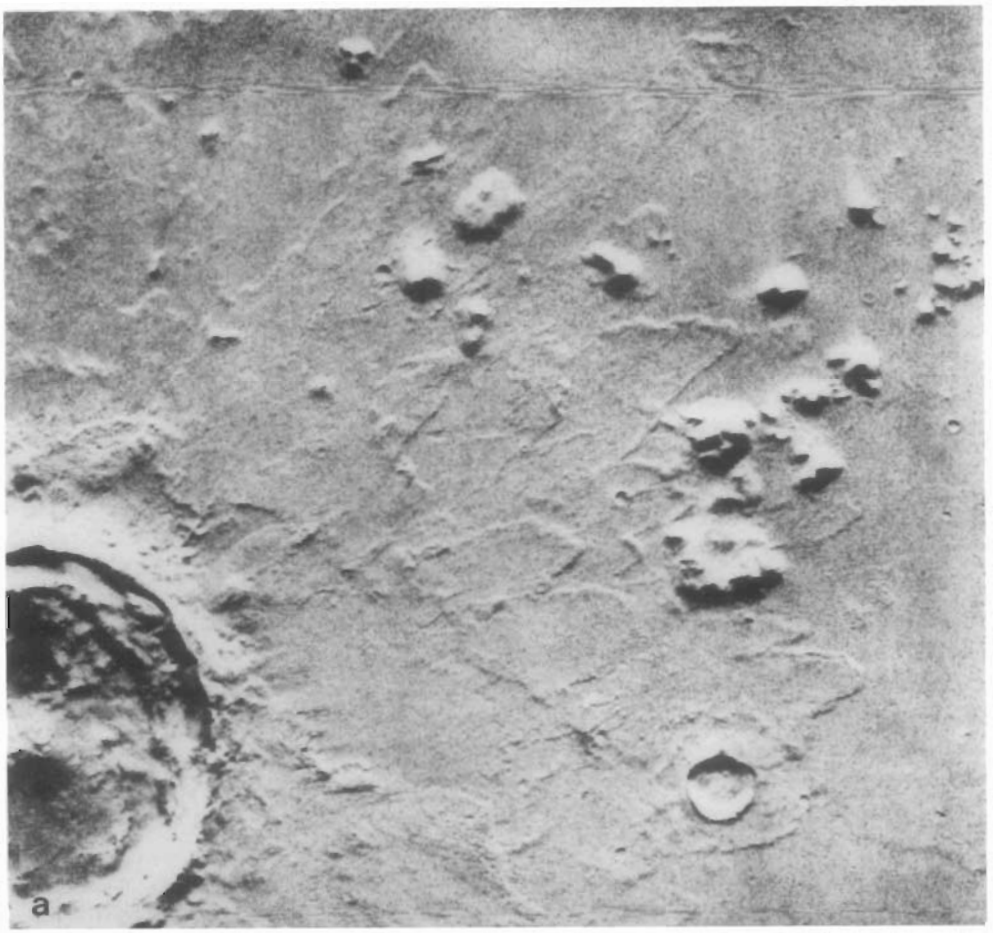

FIG. 4. Paired photo (a) and map (b) showing the effect of small hills on the distribution of rampart ejecta. Lobe L_1 was blocked by some hills, passed through some saddles, and was channelized into a long runout stream where flow was confined. Viking image 220A20.

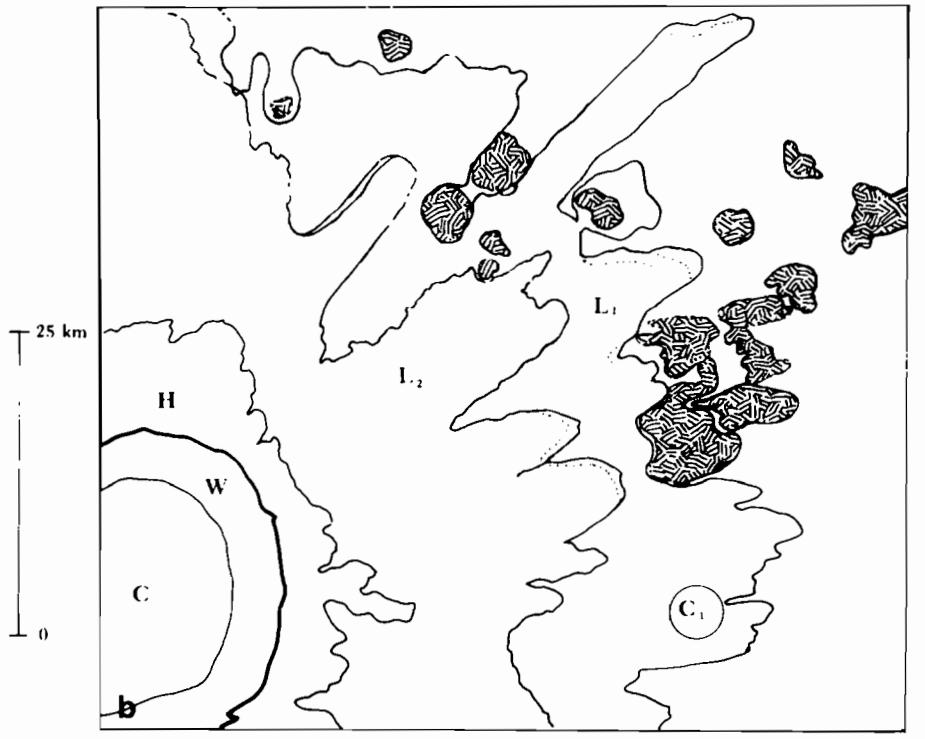

FIG. 4—*Continued.*

topographic rim of C_1 leaving a thin mantling deposit but that L_3 was deflected around C_1 suggests that the earlier flows were of higher energy. Hummocky material (H) from Yuty also appears to have deflected around the topographic rim of C_1, with some of this material spilling over the rim of C_1 to cover the crater floor. These features demonstrate the strong effect of topography on the distribution of ejected material.

A 28-km-diameter crater (Figs. 3a and b) has two distinct lobe sets, each with a well-developed outer rampart. L_1 has spread onto a low plateau region, but abuts against the highlands near the bottom of the map. This observation demonstrates the ability of ejecta lobes to overtop low topographic barriers but not high mountain ranges. Ramparts did not form where the highlands caused the flows to pond before reaching their maximum runout distance. Wind streaks, apparently adjacent to small fresh craters in the plains, are also observable along the margins of L_1. The proximity of wind streaks to L_1 suggests that this rampart lobe consists of unconsolidated particles that were readily transported by Martian winds.

A 17-km-diameter crater (Figs. 4a and b) has an extensive apron with distinct terminal terraces but poorly defined interior lobes. The small group of hills in the upper part of the photo were a strong topographic control on the distribution of flow lobes L_1. High ridges have blocked the flow, saddles have allowed passage without deposition, and plains beyond gaps in the hills have provided runout chutes for flow lobes.

Relationships recorded on these maps constructed from Viking images include: (1) Emplacement of outer lobe sets occurs before inner lobe sets. (2) Outer lobes may pass over higher topographic barriers than inner lobes. (3) Distribution of hummocky material is also topographically controlled. (4) Lobes that pond where they abut against existing topography lack ramparts. (5) Flow

ejecta deposits are composed of unconsolidated, fine-grained particulate matter that can be retransported by Martian winds. (6) Flows that are channelized through gaps in topography may attain increased runout. (7) Flow lobes may run into and out of topographic depressions leaving only a thin deposit without complete ponding and spillover.

The details of rampart lobe distribution and morphology provide additional insight into their emplacement. Lobe set perimeters seem to be continuous, albeit undulating, which suggests that each lobe set (L_1, L_2, L_3, etc.) originates from an individual ejecta pulse of a characteristic transport energy. Scalloping is greater for the outer ring lobes (L_1) than for inner lobes (L_2 and L_3). The rampart width of the outer lobes is likewise greater than that for inner lobes indicating that their flow continued for a longer distance after the development of yield strength in the flows.

EXPERIMENTATION

Vapor explosions resulting from the interaction of a molten fluid with water are usually termed "fuel–coolant interactions" (Colgate and Sigurgeirsson, 1973; Peckover *et al.*, 1973; Corradini, 1981). As mentioned earlier, this process has attracted much study due to its devastating affects in steel foundaries and its potential hazard in the event of nuclear reactor core meltdown (Sandia Laboratories, 1975). The rapid conversion of thermal to mechanical energy and the remarkable efficiency of the process are still poorly understood even after numerous laboratory studies (Sandia References). This phenomenon is similar to phreatomagmatic explosions which produce maar volcanoes (Wohletz, 1980; Heiken, 1971; Lorenz, 1973; Ollier, 1967).

Our first series of experiments at Los Alamos National Laboratory were designed to document the phenomenology of this process on a larger scale than past investigations in order to assess its affects upon planetary cratering. Approximately 100 kg of thermite was ignited to form a melt of similar physical properties as those of basalt. This melt is brought into contact with water within a steel confinement chamber. The Series I chamber (Fig. 5) is equipped with a vent designed to burst at predetermined pressures. The confinement chamber is monitored by continuously recording pressure and temperature gauges. The mass of water contacting the melt, burst pressure, and contact geometry have been varied in this series of experiments. High-speed cinematography is used to record the phenomenology of the vapor explosion during venting.

A representative experiment with a water–melt mass ratio of about 0.20 was performed in December, 1980 (Figs. 6 and 7). Our main purpose was to analyze the explosion characteristics and the interaction of ejected melt fragments with the external flow field produced by the expanding volatile cloud. Larger fragments follow unmodified parabolic paths, whereas small-sized ejecta experience significant aerodynamic drag due to their interaction with the atmosphere and superheated steam. The drag turbulence causes separation of fine particles from the ballistic plume. This separated material collapses as a density cloud (surge) and flows horizontally away from the crater (Fig. 6).

Although the cratering mechanism for this experiment is quite different from that of an impact event, the deposit morphology (Fig. 7) resembles that associated with small chemical explosions and small-scale Martian craters observed on Viking images. Data on the resulting deposit (Table I) show that 65% of the total displaced mass lies within two crater radii. This mass distribution is similar to that observed by Stoffler *et al.* (1975) for deposits formed by ballistic transport due to impact of projectiles into dry sand. This result shows that there is little difference in morphology between deposits formed by small-scale melt–water explosions and those related to impact and explosion cratering in dry material. How-

FIG. 5. Steel vessel used in the thermite–water experiments. Note the connectors for *P–T* readout. A Kodak film box is shown for scale.

ever, an increase in the mass ratio above 0.20 drastically increases vapor expansion and ejecta runout as observed for large, Martian rampart craters (Mouginis-Mark, 1979a).

Since the excavation dynamics of the experimental vapor explosions are quite different from those of impact origin, our focus centers on the properties of the vapor-particulate cloud that collapses after impact crater formation. Important parameters are: size, velocity, and trajectories of particles, as well as the physical state of the vapor (i.e., condensing, saturated steam vs expanding, superheated steam). These parameters have been shown by experiments

FIG. 6. Ejection plume for water thermite experiment. Note the vertical column of coarse ballistic particles (A) and the low cloud of fine surge particles (B) that is starting to move laterally.

FIG. 7. A close-up photograph depicting the crater and morphology of ejecta deposits formed by the experiment shown in Fig. 6. The crater is 2.13 m in diameter and extends 0.33 m below the ground surface. Ejecta is 0.27 m thick at the rim and is continuous to about 5 m from the crater rim. Collection boards 0.6 m on a side were placed at 1-m intervals away from the crater to collect ejecta. Vertical plates were blown over by the surge to a distance of about 5 m from the crater rim.

TABLE I

MORPHOLOGY AND DISPLACED MASS OF EXPERIMENTAL CRATER

Radius (m)	Area (m^2)	Thickness[a] (cm)	Mass/board[b] (kg)	Total mass (kg)
0.00–0.66	1.36	0.00	—	0
0.66–0.81	0.70	15.00	—	110
0.81–0.97	0.89	30.00	—	356
0.97–1.12	0.99	29.00	—	426
1.12–1.27	1.12	26.00	—	489
1.27–1.42	1.27	20.00	—	484
1.42–1.58	1.51	16.00	—	547
1.58–1.73	1.56	11.00	—	402
1.73–1.88	1.70	7.00	—	303
1.88–2.03	1.85	3.00	—	154
2.03–2.19	2.11	0.50	—	34
2.3–3.3	17.61	2.55	13.78	674
3.3–4.3	23.87	1.14	6.14	407
4.3–5.3	30.86	0.67	3.64	305
5.3–6.3	36.46	0.38	2.05	208
6.3–7.3	42.70	0.08	0.45	53
7.3–8.3	49.00	0.02	0.12	16
8.3–9.3	55.80	0.01	0.3	5

[a] Thickness is calculated from mass collected on boards (2.3–9.3 m).
[b] Collection boards are 0.36 m^2.

(Wohletz and McQueen, 1981) to be strongly influenced by the mass interaction of water and melt (Fig. 8).

Ejection phenomenology can be compared with mechanical energy efficiency calculations (Table II) based on pressure records from four experiments. A Redlich–Kwong equation of state is used instead of a Murnaghan equation (Kieffer and Simonds, 1980) in order to better approximate the P–V relationships of a water-rich system. More detailed descriptions of this experimentation are given by Wohletz and McQueen (1981, 1983) and Wohletz (1980). The efficiency of conversion of melt thermal energy to mechanical energy of ejectamenta is a function of water–melt ratio (Fig. 9). An increase in water interaction causes greater melt fragmentation; associated vaporization results in high-energy surges. The maximum degree of superheating and melt fragmentation for thermite occurs for mass ratios between 0.3 and 0.6.

The mode of particle transport is directly related to particle size, especially if aerodynamic drag effects are important. Size data from samples produced by naturally occurring steam explosions at terrestrial volcanoes (Sheridan and Wohletz, 1983) relate three main groupings; (1) ballistic, (2) dry surge, and (3) wet surge to the dominant eruption mode (Fig. 10). These groups, which are a function of water–melt interaction, have a direct bearing on rampart crater ejecta morphology.

The systematics of magma–water interaction has only recently been investigated. Studies in progress (Sheridan and Wohletz, 1981; Wohletz and Sheridan, 1983) of small terrestrial volcanoes show a strong correlation among deposit morphology, particle size, and eruption mode related to various degrees of water interaction. Products range from cinder cone (ballistic), through tuff rings (dry surge), to tuff cones (wet surge). Interaction of water with basaltic magma at small mass ratios (H_2O/melt less than 0.10) produces cinder cones composed of centimeter-sized, ballistic clasts that followed parabolic trajectories. Highly explo-

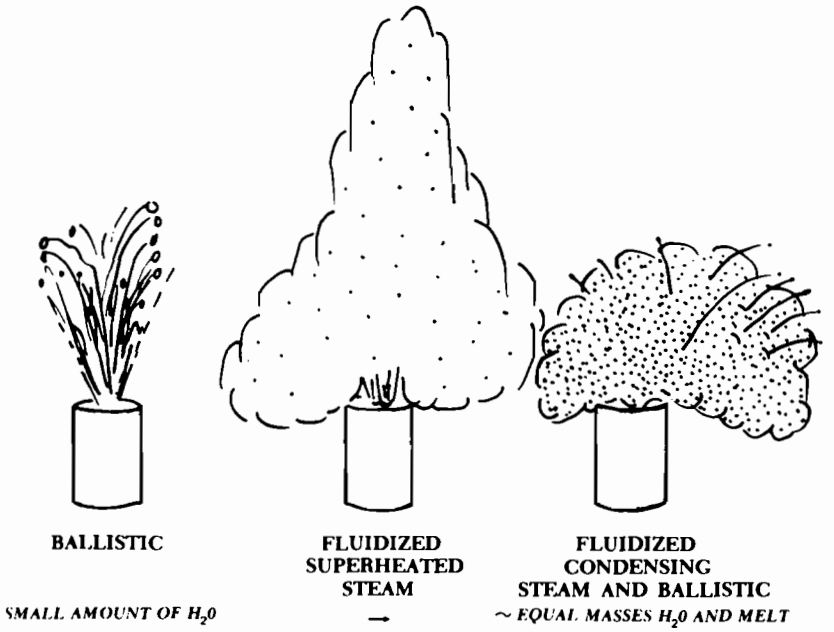

FIG. 8. Phenomenology of water–thermite experiments. As the ratio of water to melt increases the ejection changes from ballistic to clouds of fine-surge clasts to sputtering emission of coarse and fine clasts in weak surge-like explosions.

sive interactions with mass ratios from 0.1 to 1.00 create tuff rings composed of micron-sized particles transported to extreme run-out distances by low-density surges with dry, superheated steam. Less explosive interactions with mass ratios above 1.00 produce tuff cones of millimeter-sized particles that are deposited from dense surges with wet, saturated steam. We speculate that ballistic, dry surge, and wet surge deposits

TABLE II

THERMITE–WATER EXPERIMENTAL SUMMARY

Water–melt ratio	Approximate efficiency[a] (% of maximum)	Ejecta size (cm)	Pressure[b]	Transport
A. 0–0.2	<10	10^{0}	10^{0}–10^{1} sec, <100 bar	Ballistic
B. 0.2–1.0	10 to 100	10^{-4}	10^{-3} sec, >220 bar	Fluidized in superheated steam
C. 1.0–10.0	10 to 20	10^{-2}	10^{0}–10^{1} sec, 0–220 bar	Fluidized in condensing steam and ballistic
D. >10.0	<1	10^{1}	10^{2} sec, 0–40 bar	Fluid flow

[a] Efficiencies—ratio of mechanical to thermal energy calculated as percent of the thermodynamic maximum for fuel–coolant explosions.

[b] Duration and magnitude of pressure pulse.

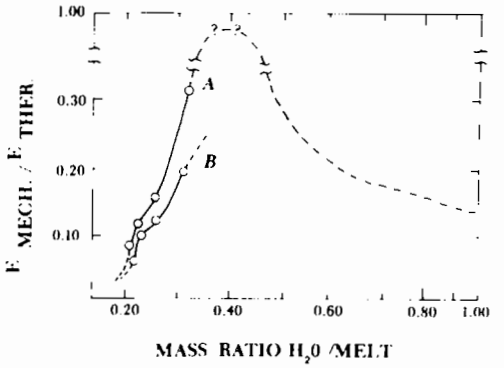

FIG. 9. Efficiency vs mass ratio for water–melt experiments. Dashed line shows the inferred projection of the efficiency curves. Curve A represents superheating and curve B is for nonsuperheating.

could correspond to lunar-type, lobate-type, and pedestal-type ejecta blankets observed on other planetary surfaces.

FLUIDIZATION

Fluidization has been used in the literature in reference to a wide spectrum of processes involving the mass flowage of particulate materials. For our purpose we define fluidization as "a mixture of particles (solid or liquid) suspended by an upward moving fluid (liquid or gas) such that the frictional force between the fluid and particles balances the weight of the grains and the whole mixture behaves like a fluid." This definition has been adapted to current analyses of pyroclastic flow emplacement (for example: Sparks, 1976; Wilson, 1980). However, it does not include target fluidization which results from acoustic and seismic energy present in the material surrounding the crater after impact (Schultz and Gault, 1975; Melosh, 1979; 1982). As natural fluidized systems move laterally, the upward fluid flux generally decreases with time and distance. Concurrently, the frictional resistance among grains and the substrate increases. This friction slows lateral movement and eventually brings the flow to rest.

Laboratory experiments have been conducted to determine the upward velocity of expanding gases required to fluidize pyroclasts in the size range produced by vapor explosions (Sheridan, 1979; Sparks, 1979; Wilson, 1980). As expected, the experimental minimum fluidizing velocity on Earth increases with grain size (Fig. 11). The required velocities would be much less on Mars than on Earth because of the reduced gravitational field. Particles in the size

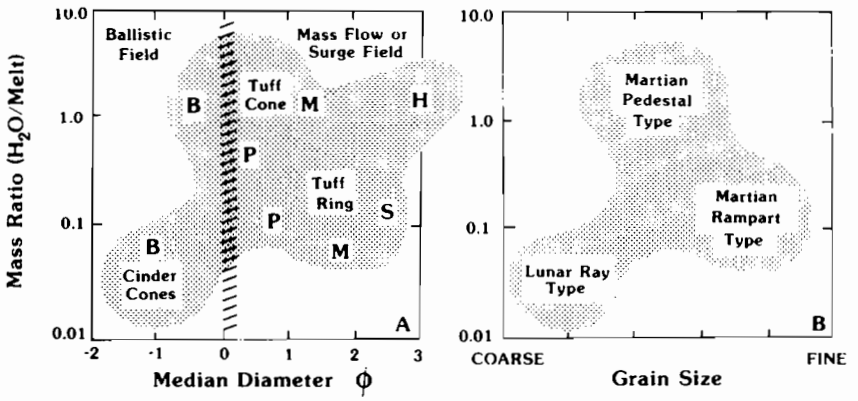

FIG. 10. Plots of water–melt mass ratio versus grain size. Data are from inferred terrestrial volcanic analogs and show grain size regions for ballistic emplacement and vapor supported surge transport, where B = ballistic emplacement typified by growth of cinder cones (McGetchin *et al.*, 1974); P = planar surge; M = massive surge; S = sandwave surge; H = hummocky material. Tuff cones consist of wet surge products characterized by planar and massive deposits and tuff rings consist of dry surge products which are sandwave and massive surge. These volcanic ejecta morphologies are related to impact ejecta morphologies in the right-hand diagram.

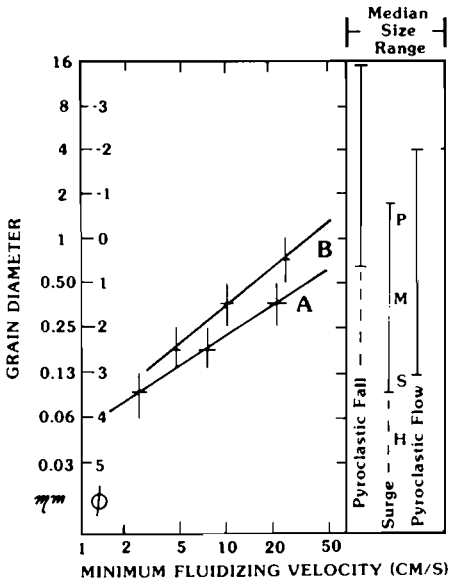

FIG. 11. Relationship of grain size to minimum fluidizing velocity of pyroclasts on Earth (from Sheridan, 1979).

range produced by maximum-efficiency steam-blast explosions (1 to 50 μm) can be fluidized by a modest upward expansion velocity. These velocities of steam relative to that of particles probably exist near the crater by superheated steam expansion.

The effects of fluidization upon transport of particulate materials have been studied extensively in industrial processes (for example, Leva, 1959; Kunii and Levenspiel, 1969). These basic principles have been applied to geologic phenomena (Reynolds, 1954; Sparks, 1976; Wohletz and Sheridan, 1979). The columns in Fig. 12 show particle separation for three degrees of fluidization. In column A, particles are barely separated at the incipient level of fluidization where void space (Φ) is 60%. Grains are sufficiently close so that flow energy is transmitted by grain collisions (inertial effects) and nonfluidized, laminar flow results. Resulting deposition is related to traction load or avalanching flow of particles and produces planar deposits with inverse grading. Such flows have a finite yield strength that produces flow front scarps (ramparts and levees). In column C particles are separated by a high degree of fluidization where void space (Φ) is greater than 90%. In this example the viscous effects of the interparticle gas dominate over inertial effects of the particles. Saltating viscous flow of particles bouncing over a substrate results in development of dunes similar to desert dunes studied by Bagnold (1954a,b). An initial highly fluidized ejecta cloud (column C) will lose fluidizing gases (defluidize) as it flows away from the crater and pass through an intermediate state (column B) where viscous and inertial forces are nearly equal. Resulting deposits are hummocky and noncontinuous due to clots of particles segregating in the flow and falling out of the cloud to form mounds [see "clot slugging" (Leva, 1959)].

PARTICULATE DISPERSAL

Grain size has a critical effect on the mechanism of transport and deposition in fluidized systems. True fluidization affects only a restricted range of particle sizes which approximate three size classes for terrestrial ash flows (Sparks, 1976). Elutriation is a common feature of fluidized systems when the upward velocity of the fluid is greater than the downward terminal fall velocity of particles in that medium (Kunii and Levenspiel, 1969). The smallest particles, elutriated from the top of a flow by the escaping fluid, may be carried away as a

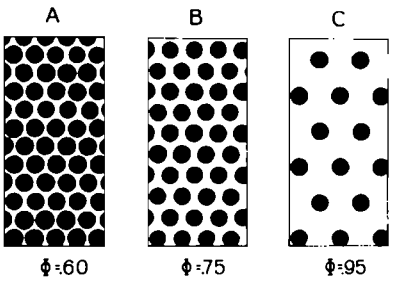

FIG. 12. Grain dispersal in flows of various types. (A) Grain flow during rampart formation. (B) Quasi-fluidized flow prior to rampart formation. (C) Dispersed viscous flow in surge clouds proximal to the crater.

dilute suspension in an overriding cloud. Particles that are too large to be fluidized may sink, float, or be transported depending on their density and the Reynolds number of the flow.

Fluidization enhances viscous transport and grain-flow (inertial flow), although the latter can occur in a vacuum. Grain-flow (Bagnold, 1954, 1956; Hsu, 1978) refers to movement of cohesionless particles under the influence of gravity in which the flow energy is transmitted through the collisions of grains. The range of particle concentration in grain flow may be sufficient to duplicate the bed forms exhibited by fluidized transport. For this reason an atmosphere is not necessary for the formation of patterned ejecta deposits produced by surge flowage although it is necessary to produce the massive flow of Schultz and Gault (1979). In viscous flow, common to terrestrial fluviatile systems, grains are transported due to shear and buoyancy stresses exerted by the moving fluid medium.

From the preceding discussions, ejecta dispersal may be classified as ballistic, grain-flow, or fluidized. Schultz and Gault (1979) describe ballistic emplacement in which the largest fragments follow parabolic paths with little atmospheric effect. Intermediate-sized particles follow ballistic paths strongly affected by atmospheric drag due to a greater surface area to mass ratio. Small particles, however, may become fluidized by rapidly expanding gasses or entrained in grain flow. During fluidized transport, the finest-sized population of particles may be removed from the ejecta flow by elutriation and transported by suspension in a cloud. Particles traveling at high velocities parallel to the ground surface may move by grain flow if there is little or no fluidization. Viscous transport of these particles occurs if an intergranular fluid transmits sufficient lateral shear stress to cause particle motion. Thus, during and after crater excavation of wet targets several intergradational processes may occur. Initially, ballistic and fluidized transport occurs during expansion of the heated vapor. The role of fluidization diminishes outward from the crater as the fluid (steam) is lost or condensed so that the main part of transport is incipiently fluidized. By the terminal stage of emplacement the system is best described as laminar grain flow or viscous transport, depending on the content of entrained fluid.

SURGE MECHANISM

Several recent papers on volcanic base surges, pyroclastic surges, or gravity-driven density flows have a bearing on our model for emplacement of vapor-modified ejecta sheets on Mars (Waters and Fisher, 1971; Wohletz and Sheridan, 1979; Fisher, 1979; Reimers and Komar, 1979). Surge transport has been defined (Wohletz and Sheridan, 1979) as a "time-transient, unsteady horizontal flow of particles and gas that occurs as a pulse or series of pulses in which the kinetic energy rapidly decays." If sufficient kinetic energy is transferred by grain-to-grain collisions an interparticulate fluid phase is not necessary for flowage of a cohesionless mass of solid fragments, such as a landslide (Heim, 1932; Hsu, 1978). As in the case of industrial grain flows, the spacing of particles necessary to allow mobility is caused by the net dispersive pressure due to the kinetic energy of particle collisions (Bagnold, 1954; 1956).

Viscous, drag effects of an interparticulate fluid on grains is important in fluidized systems (Kunii and Levenspiel, 1969) and in natural fluid transport of grains as slurrys or dilute grain dispersions. In high-concentration flows (Fisher, 1971) the void fraction or particle concentration per unit volume can strongly affect such important fluid properties as viscosity and yield strength. Thus, a surge pulse having a high velocity and low viscosity is turbulent at high void fractions and will approximate Newtonian behavior. Frictional forces affecting particle motion increase in significance with decreasing void fraction. This produces a higher viscosity with a finite

Bingham yield strength, so that, with increasing particle concentration, flows become laminar and nonNewtonian (Sheridan and Updike, 1975; Wilson, 1980).

Our model of rampart ejecta emplacement (Fig. 1) assumes that the initial parabolic trajectories of ejected particles may be strongly modified by aerodynamic drag. Because this drag effect dramatically increases as the grain size decreases (Schultz and Gault, 1979), ballistic fragments less than a few millimeters in diameter are limited to low-altitude paths during excavation of Martian craters. If sufficient fine material is produced, it would collapse downward as a density flow. As this turbulent mixture of fine particles and vapor reaches the ground, it spreads outward as a horizontally surging cloud driven by the force of gravity (Young, 1965). Explosive melt–water interaction causes a series of pulses as demonstrated by drop size and large (100 kg) experiments (Nelson and Duda, 1981; Wohletz and McQueen, 1981). Larger explosions produced by the interaction of magma and sea water likewise are pulsing. The frequency of explosive pulses is dependent upon system size. Experimental frequencies are on the order of micro- to milliseconds, whereas volcanic systems display pulse frequencies of minutes. For this reason, vapor explosion during Martian crater excavation would probably produce multiple surges that decrease in energy with time and distance from the crater. As these turbulent mixtures of fine particles and vapor collapse to the ground, they develop into horizontally surging clouds that are essentially driven by the force of gravity. Continued vapor explosions and collapses during crater excavation would produce multiple surges that decrease in energy with time and distance from the crater.

The surges initially move as dilute, viscous flows from which the suspended and saltating grains are deposited, particle by particle, in thin beds that mantle the existing topography. As fluidization levels in the surges drop below a critical value with distance, the resulting increase in their particle concentration causes a change to inertial grain flow with a finite yield strength. During this transition from viscous to grain-flow motion, deposition occurs en masse producing thick deposits that pond and are strongly affected by topography. Flow lobes terminate in ramparts at this stage. Laboratory fluidization experiments (Wilson, 1980) and field studies (Sparks, 1976; Wright, 1979; Wright and Walker, 1981) support the above conclusion. Partially fluidized particulate flows, such as pyroclastic flows, do not slow down gradually, but suddenly decelerate to a halt (Wolf and Wright, 1981), producing prominent flow scarps.

ENERGY LINE

A simple heuristic model of surge ejecta emplacement can be formulated based on gravity-driven dispersal controlled by an energy line (Sheridan, 1982). A detailed description of the energy line model is given by Hsu (1975, 1978). Hsu explains mass transport of landslide material by grain flow. His model also is useful in analyzing emplacement of pyroclastic flows (Sheridan, 1979) and steam-blast explosions (Sheridan, 1980). The principal assumption is that an energy line can be drawn connecting the highest elevation of the material before flowage to the toe of the resulting deposit. The Heim (1882) constant (tangent of the energy line slope, μ), gravitational acceleration (g), and the configuration of the underlying topography are sufficient constraints to permit calculation of the main flow parameters. The elevation of the energy line above the ground surface (Δh) defines the velocity potential (v_p),

$$v_p = (2g\Delta h)^{1/2}. \quad (1)$$

The horizontal acceleration (a_x) is a function of the topographic slope (β) and the Heim constant (μ) (Hsu, 1978),

$$a_x = g(\sin \beta - \mu \cos \beta). \quad (2)$$

The velocity and runout times for any part

of the flow field can be calculated by equations given by Hsu (1978).

For example, apply the model to a 20-km-diameter Martian crater with a rampart lobe extending 30 km from the rim. The bulk of the particles comprising the rampart ejecta deposit are probably less than 250 μm in diameter, assuming high fragmentation caused by the presence of the water. The Martian atmospheric drag on grains less than 1 cm diameter would limit the vertical ballistic elevation to less than one-half the crater radius which in this case would be 5 km (Schultz and Gault, 1979). A gravity collapse of a density cloud from this height yields a potential velocity of about 200 m/sec. Assuming a level runout surface, the deceleration of the cloud would be -0.6 m/sec^2 and the minimum runout time would be about 300 sec.

This model can be applied to more complicated three-dimensional situations by constructing an appropriate energy surface instead of an energy line for the three-dimensional field. From the potential velocity, a first-order flow field can be calculated assuming steady, nonviscous flow. Because of the sensitivity of flows to topography, the limiting constraints for optimum application of the model to an analysis of rampart ejecta is the availability of adequate topographic base maps.

DISCUSSION

Consideration of the rampart ejecta maps, the experimental work, and observations of terrestrial deposits of vapor explosion origin allows the following illustrations of the model to be put forth (Fig. 13). This figure incorporates the aspects of fluidized transport and maintains that ramparts and terraces are deposited as a result of the transition from quasi-fluidized viscous ejecta to inertial fixed-bed emplacement.

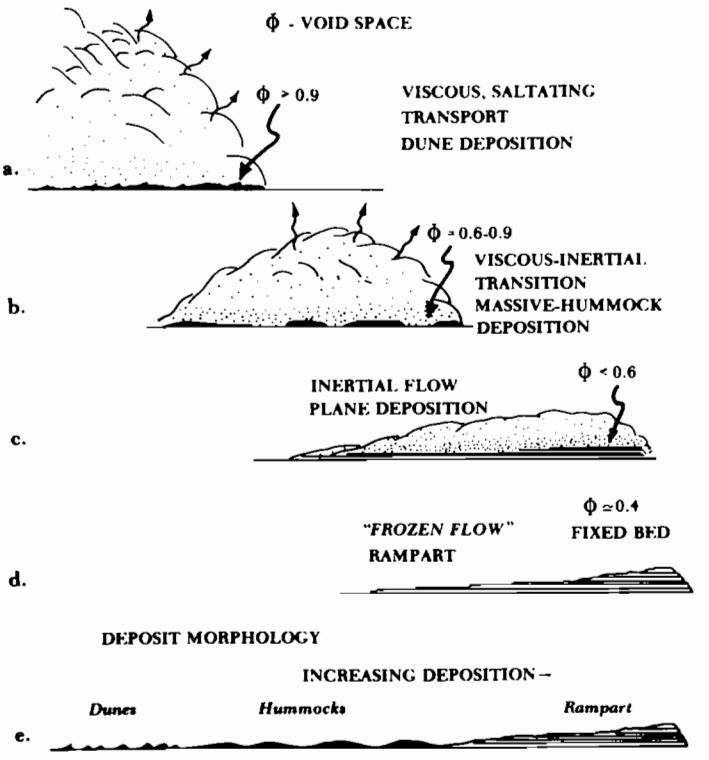

FIG. 13. Detailed model of rampart ejecta emplacement.

Figure 13 (a–d) illustrates the development of deposit morphology by fluidized transport of ejecta (stages 3 and 4 shown in Fig. 1). A facies distribution develops with dunes or ridges of ejecta near the crater, thin hummocky deposits at intermediate distances from the crater, and gradually thickening planar deposits with distal ramparts (Fig. 13e) at the limits of continuous ejecta deposits. Repeated vapor explosion pulses during and after crater excavation produce multiple lobes that obscure the proximal ejecta morphology and result in overlapping ramparts. Consolidation of the deposits is primarily dependent upon the degree of post emplacement ejecta alteration (Wohletz and Sheridan, 1981).

Findings of the Viking lander (Toulmin *et al.*, 1977) suggest that much of the Martian surface material is composed of hydrated silicate or clays. Hydration of ejecta from vapor explosions in impact events (Kieffer and Simonds, 1980) is expected. The degree of hydration depends upon the wetness of ejecta during and after emplacement. The amount of water trapped in a deposit after emplacement depends upon the degree of segregation of volatiles from particles during emplacement. If steam is highly superheated during transport, the tendency of segregation of the steam from the particles is increased and deposits will be dry. On the other hand, if steam is saturated during transport, much of it will condense on ejecta particles resulting in wet deposits subject to postemplacement hydration. The experimental curve of Fig. 9 is shown in Fig. 14 with a dry and wet division. Increasing water–melt ratios in the dry region results in higher melt fragmentation, higher rates of thermal energy release from melt to the water, and increased vapor superheating. In the wet region, however, increasing water–melt ratios will quench the melt because of the excess total heat capacity of the water. Steam produced becomes increasingly cooler and water droplets larger. The division between wet and dry is of course gradational, and dependent upon the melt enthalpy and the degree of confinement in the area of interaction.

The result of wet and dry vapor explo-

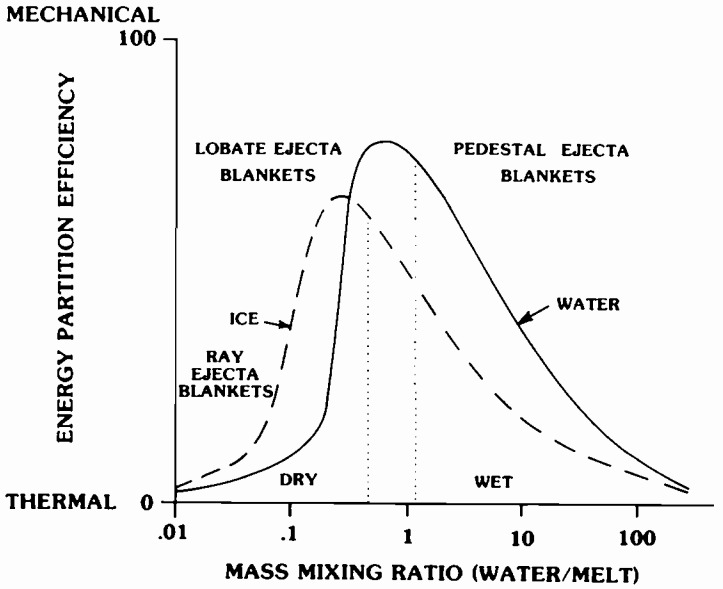

FIG. 14. Partitioning of thermal and mechanical (0–100%) emplacement energy to the water–melt ratio. The wet (water, steam, clast) field and the dry (steam, clast) field are shown as well as curves for water and ice. The partition values are approximated and mixing ratios are calculated from thermite–melt experiments.

sions upon ejecta morphology is summarized in Fig. 15. Impacts into a dry target generally result in dominantly ballistic emplacement of ejecta with subsequent atmospheric effects that may limit the range of continuous ejecta deposits. An increase in the mass ratio of water to impact melt in the zone of excavation increases the effect of fluidized transport. Flow emplacement occurs where target water abundance produces high-energy vapor explosions. These target areas are characterized by the formation of ramparts and maximum ejecta runout. Water contents in excess of that needed for high-energy vapor explosion result in wetter, less-fluidized flows with increasing cohesion. Still wetter conditions tend toward ejecta terrace formation and a diminished runout distance. The tendency for formation of terraced ejecta deposits of relatively short runout distances should be expected where target water is in the form of ice. This is because of the increased heat needed to vaporize ice over that required for liquid water. Hence, maximum, explosive heat exchange occurs at lower water–melt mass ratios in an icy terrain. For a water-rich Martian crust of constant water content (near the explosive maximum), terraced, stuby ejecta flow deposits are expected to form at higher latitudes and altitudes where water is ice. This result is supported by Mouginis-Mark (1979a) who shows preliminary data indicating that pancake (type 6) craters are more common in high latitude and altitude areas and that craters with ejecta runout distances (ER) of 0 to 4 crater radii are favored in lower latitudes. However, Mouginis-Mark (1979a) also demonstrates that high latitudes are fa-

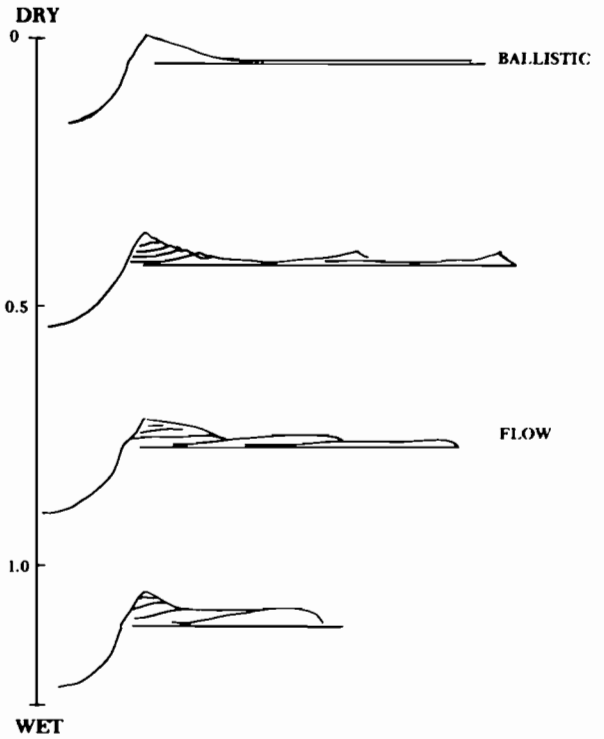

FIG. 15. Schematic profile of ejecta blankets showing the relationship of deposit morphology to water content of the target material. Water contents are shown on the vertical axis as mass ratio of water to melt in the zone of target melting. The runout distances of ejecta shown are variable and scaled approximately to crater radius.

vorable for ejecta runout distances greater than 4. This suggests that strongest ejecta fluidization may occur in areas where the optimum water–melt ratio is controlled by water in the form of ice. In other words, the presence of ice shifts the efficiency curve peak nearer to the water–melt ratio of water-poor targets.

CONCLUSIONS

Much of our present understanding of the evolution of planetary bodies is based upon studies of meteorite impacts. Comparative analysis of impact structures on Moon and Mercury with those of the Earth and Mars strongly supports the hypothesis that surface water can greatly influence the impact process. Existence of ejecta showing evidence of surface flow such as lobate margins, ramparts, and terraces, cross-cutting relationships, topographic effects, and multistratigraphic deposits around craters suggests emplacement as fluidized flows. Studies of terrestrial fluidized flows of particles as well as industrial fluidization processes provide adequate analogs to interpret the emplacement process. Experiments dealing with the explosive interaction of thermite melt and water show that the mass ratio of water to melt and the degree of confinement in the zone of interaction strongly affect the emplacement of ejecta. Important factors of emplacement of ejecta fluidized by vaporized water are the size population of particles, the physical state of the volatile substance (condensing–saturated or superheated–expanding steam) and the level of ejecta cloud fluidization (the volume ratio of gases to particles).

We conclude that water either on or beneath the surface of Mars interacted with impact melt during crater excavation to produce vapor explosions. These explosions altered initial parabolic trajectories of ejecta to form partly fluidized flows that deposited the rampart and terraced ejecta, a conclusion in agreement with Schultz and Gault (1979). Furthermore, the water-to-melt ratio in the zone of crater excavation determined the degree of vapor expansion and melt fragment size. The movement of the resulting vapor-fluidized ejecta clouds followed a predictable path where initially viscous flows decrease in energy and degree of fluidization as they move away from the crater. At the distance from the crater where flows were deflated below the critical fluidizing level, deposition of ramparts began en masse as the shear stress of the flow decreased below the yield strength. Terraced deposits resulted from poorly fluidized ejecta moving in laminar flows away from craters. The morphology of Martian impact craters is therefore strongly related to the physical state and amount of water present in the crust at the time of impact.

ACKNOWLEDGMENTS

Robert McQueen directed and provided technical support for the experimental work. Ronald Greeley encouraged our research in impact ejecta emplacement and provided Viking imagery as well as technical advice on cratering mechanisms. Financial support from NASA Grants NSG-7642 and NAWG-245 is gratefully acknowledged.

REFERENCES

BAGNOLD, R. A. (1954a). *The Physics of Blown Sand and Desert Dunes*. Methuen, London.

BAGNOLD, R. A. (1954b). Experiments on a gravity-free dispersion of large-solid spheres in a Newtonian fluid under shear. *Proc. R. Soc. London* **225**, 49–63.

BAGNOLD, R. A. (1956). The flow of cohesionless grains in fluids. *Phil. Trans. R. Soc. London* **249**, 291–293.

BLASIUS, K. R., AND J. A. CUTTS (1980). Global patterns of primary crater ejecta morphology on Mars. *NASA Tech. Memo.* **82385**, 147–149.

CARR, M. H., L. S. CRUMPLER, J. A. CUTTS, R. GREELEY, J. E. GUEST, AND H. MASURSKY (1977). Martian impact craters and emplacement of ejecta by surface flow. *J. Geophys. Res.* **82**, 4055–4065.

CARR, M. H., AND G. S. SCHABER (1977). Martian permafrost features. *J. Geophys. Res.* **82**, 4039–4054.

CINTALA, M. J., AND P. J. MOUGINIS-MARK (1980). Martian fresh crater depth: More evidence for subsurface volatiles? *Geophys. Res. Letters*, **7**, 329–332.

COLGATE, S. A., AND R. SIGURGEIRSSON (1973). Dynamic mixing of water and lava. *Nature* **244**, 552–555.

CORRADINI, M. L. (1981). Phenomenological modeling of the triggering phase of small-scale steam explosion experiments. *Nucl. Sci. Eng.* **78,** 154–170.

FISHER, R. V. (1971). Features of coarse-grained, high concentration fluids and their deposits. *J. Sediment. Petrol.* **41,** 916–927.

FISHER, R. V. (1979). Models for pyroclastic surges and pyroclastic flows. *J. Volcanol. Geotherm. Res.* **6,** 305–318.

GAULT, D. E., AND R. GREELEY (1978). Exploratory experiments of impact craters formed in viscous-liquid targets: Analogs for Martian rampart craters? *Icarus* **34,** 486–495.

GREELEY, R., J. FINK, D. E. GAULT, D. B. SNYDER, J. E. GUEST, AND P. H. SCHULTZ (1980). Impact cratering in viscous targets: Laboratory experiments. *Proc. Lunar Plan. Sci. Conf. 11th,* 2075–2097.

HEAD, J. W., AND R. ROTH (1976). Mars pedestal crater escarpments: Evidence for ejecta-related emplacement. In papers presented to the *Symposium of Planetary Cratering Mechanics,* pp. 50–52. The Lunar Science Institute, Houston, Tex.

HEIKEN, G. H. (1971). Tuff rings: Examples from Fort Rock–Christmas Lake Valley, south-central Oregon. *J. Geophys. Res.* **76,** 5615–5626.

HEIM, A. (1882). Der Bergsturz von Elm. *Z. Deutsch Geol. Ges.* **34,** 74–115.

HEIM, A. (1932). *Bertsturz und Menchenleben.* Fretz and Wasmuth, Zurich.

HSU, K. J. (1975). On sturzstroms—Catastrophic debris streams generated by rockfalls. *Geol. Soc. Amer. Bull.* **86,** 129–140.

HSU, K. J. (1978). Albert Heim: Observations on landslides and relevance to modern interpretations. In *Rockslides and Avalanches, Vol. 1, Natural Phenomena* (B. Voight, ed.), pp. 71–93. Elsevier, New York.

JOHANSEN, L. A. (1979). The latitude dependence of Martian splosh cratering and its relationship to water. *NASA Tech. Memo.* **80339,** 123–125.

JONES, E. M., AND J. W. KODIS (1982). Atmospheric effects of large-body impacts: the first few minutes. *Proc. Snowbird Conf., Geol. Soc. Amer. Spec. Pap.* **190,** 175–186.

KIEFFER, S. W., AND C. H. SIMONDS (1980). The role of volatiles and lithology in the impact cratering process. *Rev. Geophys. Space Phys.* **18,** 143–181.

KUNII, D., AND O. LEVENSPIEL (1969). *Fluidization Engineering.* Wiley, New York.

LEVA, M. (1959). *Fluidization.* McGraw-Hill, New York.

LIPSETT, S. G. (1966). Explosions from molten materials in water. *Fire Technol.* May, 118–126.

LORENZ, V. (1970). Some aspects of the eruption mechanism of the Big Hole Maar, Central Oregon. *Geol. Soc. Amer. Bull.* **81,** 1823–1830.

LORENZ, V. (1973). On the formation of maars. *Bull. Volcanol.* **37,** 183–204.

MCGETCHIN, T. R., M. SETTLE, AND B. A. CHOUET (1974). Cinder cone growth modeled after Northeast Crater, Mount Etna, Sicily. *J. Geophys. Res.* **79,** 3257–3272.

MELOSH, H. J. (1979). Acoustic fluidization: A new geologic process? *J. Geophys. Res.* **84,** 7513–7520.

MELOSH, H. J. (1982). A schematic model of crater modification by gravity. *J. Geophys. Res.* **87,** 371–380.

MOORE, J. G. (1967). Base surge in recent volcanic eruptions. *Bull. Volcanol.* **30,** 337–363.

MOUGINIS-MARK, P. J. (1978). Morphology of Martian rampart craters. *Nature* **272,** 691–694.

MOUGINIS-MARK, P. J. (1979a). Martian fluidized crater morphology: Variations with crater size, latitude, altitude, and target material. *J. Geophys. Res.* **84,** 8011–8022.

MOUGINIS-MARK, P. J. (1979b). Ejecta emplacement of Martian impact crater Bamburg. *Proc. Lunar Planet. Sci. Conf. 10th,* 1651–1668.

MUTCH, P., AND A. WORONOW (1980). Martian rampart and pedestal craters' ejecta emplacement: Coprates Quadrangle. *Icarus* **41,** 259–268.

NELSON, L. S., AND P. M. DUDA (1981). Steam explosion experiments with single drops of CO_2 laser-melted iron oxide. *Trans. Amer. Nucl. Soc.* **38,** 453–454.

OLLIER, C. C. (1967). Maars, their characteristics, varieties, and definition. *Bull. Volcanol.* **30,** 45–73.

PECKOVER, R. S., D. J. BUCHANAN, AND D. E. ASHBY (1973). Fuel–coolant interactions in submarine volcanism. *Nature* **245,** 307–308.

REYNOLDS, D. L. (1954). Fluidization as a geologic process and its bearing on the problems of intrusive granites. *Amer. J. Sci.* **252,** 577–613.

REIMERS, C. E., AND P. D. KOMAR (1979). Evidence for explosive volcanic density currents on certain Martian volcanoes. *Icarus* **39,** 88–110.

SANDIA LABORATORIES (1975). *Core-Meltdown Experimental Review,* SAND-74-0382. Sandia Laboratories, New Mexico.

SCHULTZ, P. H., AND D. E. GAULT (1975). Seismically induced modification of lunar surface features. *Proc. Lunar Sci. Conf. 6th,* 2845–2862.

SCHULTZ, P. H., AND D. E. GAULT (1979). Atmospheric effects on Martian ejecta emplacement. *J. Geophys. Res.* **84,** 7669–7687.

SCHULTZ, P. H., AND D. E. GAULT (1982). Impact ejecta dynamics in an atmosphere: Experimental results and extrapolations. *Proc. Snowbird Conf., Geol. Soc. Amer. Spec. Pap.* **190,** 153–174.

SHERIDAN, M. F. (1979). Emplacement of pyroclastic flows—A review. *Geol. Soc. Amer. Spec. Paper* **180,** 125–136.

SHERIDAN, M. F. (1980). Pyroclastic block flow from the September, 1976 eruption of La Soufriere Volcano, Guadeloupe. *Bull. Volcanol.* **43,** 397–402.

SHERIDAN, M. F. (1982). The energy line: A heuristic model for Martian rampart ejecta sheets. Reports of

the Planetary Geology Program, 1981–1982. *NASA Tech. Memo.* **84211.**

SHERIDAN, M. F., AND R. G. UPDIKE (1975). Sugarloaf Mountain tephra—A Pleistocene rhyolitic deposit of base-surge origin. *Geol. Soc. Amer. Bull.* **86,** 571–581.

SHERIDAN, M. F., AND K. H. WOHLETZ (1981). Hydrovolcanic explosions: The systematics of water–pyroclast equilibration. *Science* **212,** 1387–1389.

SHERIDAN, M. F., AND K. H. WOHLETZ (1983). Hydrovolcanism: basic considerations and review. *J. Volcanol. Geotherm. Res.* **17,** 1–29.

SPARKS, R. S. J. (1976). Grain size variations in ignimbrites and implications for the transport of pyroclastic flows. *Sedimentology* **23,** 147–188.

STOFFLER, D., D. E. GAULT, J. WEDEKIND, AND G. POLKOWSKI (1975). Experimental hypervelocity impact into quartz sand: distribution and shock metamorphism of ejecta. *J. Geophys. Res.* **80,** 4062–4077.

TOULMIN III, P., H. K. BAIRD, B. C. CLARK, K. KEIL, H. J. ROSE JR., R. P. CHRISTIAN, P. H. EVANS, AND W. C. KELLIHER (1977). Geochemical and mineralogical interpretation of Viking inorganic chemical results. *J. Geophys. Res.* **82,** 5625–5634.

WATERS, A. C., AND R. V. FISHER (1971). Base surges and their deposits: Capelinhos and Taal Volcanoes. *J. Geophys. Res.* **76,** 5596–5614.

WILSON, C. J. N. (1980). The role of fluidization in the emplacement of pyroclastic flows. *J. Volcanol. Geotherm. Res.* **8,** 231–249.

WOHLETZ, K. H., AND R. MCQUEEN (1981). Experimental hydromagmatic volcanism. *Trans. Amer. Geophys. Union, Eos,* **62,** 1085.

WOHLETZ, K. H., AND R. MCQUEEN (1983). Experimental studies of hydromagmatic volcanism, In *Explosive Volcanism: Inception, Evolution, and Hazards* (F. R. Boyd, ed.), Studies in Geophysics, National Academy of Sciences, in press.

WOHLETZ, K. H., AND M. F. SHERIDAN (1983). Hydrovolcanic explosions II: the evolution of tuff cones and tuff rings. *Amer. J. Sci.* **283,** 385–413.

WOHLETZ, K. H. (1980). *Explosive hydromagmatic volcanism.* Ph.D. dissertation, Arizona State University, Tempe, Ariz.

WOHLETZ, K. H., AND M. F. SHERIDAN (1979). A model of pyroclastic surge. *Geol. Soc. Amer. Spec. Paper* **180,** 177–193.

WOLFF, J. A., AND J. V. WRIGHT (1981). Rheomorphism of welded tuffs. *J. Volcanol. Geotherm. Res.* **10,** 13–34.

WRIGHT, J. V. (1979). *Formation, Transport and Deposition of Ignimbrites and Welded Tuffs.* Ph.D. thesis, Imperial College, London.

WRIGHT, J. V., AND G. P. L. WALKER (1981). Eruption, transport, and deposition of ignimbrites: A case study from Mexico. *J. Volcanol. Geotherm. Res.* **9,** 11–131.

YOUNG, G. A. (1965). *The Physics of the Base Surge.* U.S. Naval Ordnance Lab., NOLTR 64-103, White Oak, Md.